

On the performance of geo-acoustic estimation for a distributed sensor array

S.M. Jesus, A. Mantouka, P. Felisberto and C. Soares
LARSyS, Universidade do Algarve Campus de Gambelas, 8005-139 Faro, Portugal
Email: {sjesus,amantouka,pfelis,csoares}@ualg.pt

Abstract—The vision underlying the Widely scalable Mobile Underwater Sonar Technology (WiMUST) project is that of developing advanced cooperative and networked control / navigation systems to enable a large number (tenths) of marine robots towing small acoustic arrays to act as a coordinated team for seismic sub-bottom imaging. The space-time coherent processing of bottom returns requires the ensemble of short acoustic arrays to be *seen* as a single spatially distributed sensor array. Since the vehicles are free to move along range, cross-range and depth the resulting distributed sensor array may take, at least conceptually, any spatial shape. With array shape freedom comes the question of which is the most suitable (or optimal) array geometry for sub-bottom imaging and inversion. The answer to this question hinges, among others, on the definition of performance of a seismic sub-bottom profiling system. Determining the optimal sensor array geometry is clearly a ill-posed problem, since the optimal geometry is itself bottom dependent, and there is no such environment as “one size fits all”. This work addresses several criteria for sub-bottom profiling system performance including gain, resolution and probability of detection. Two physical models will be tested: one based on acoustic wave reflection used in traditional seismic imaging, and another normally used in matched-field bottom properties estimation, that includes propagation and refraction. Simulations to support the theoretical developments and algorithms were obtained on a scenario inspired in a real environment off the coast of Peljesac (Croatia).

I. INTRODUCTION

Estimating ocean bottom properties poses a number of scientific and technological challenges because the media is largely anisotropic and of difficult or impossible direct access. Classical observation techniques, routinely used in the oil and gas industry since the 70s [1], [2], normally proceed in two steps: first by determining a seismic reflection image of a bottom slice or volume and then, in a second step, by inverting the data for the sub-bottom physical properties (known as migration). The first step is data massive and highly automatized, while the second step is, to great extent, user supervised and incorporates a substantial amount of *in situ* measurements and a priori information, when available.

In parallel, the scientific community has been working on alternative/complementary methods for bottom parameter estimation that involve seismo-acoustic propagation models that suitably describe the received data [3]–[5]. There is an extensive literature on the subject with many variations on the environmental settings (shallow or deep water), range independent or range dependent [6], single sensor, vertical or horizontal arrays [7], model type, that can be numerical or analytic, etc. The common trend is that these methods tend to

involve the maximization of the match between the received data and the model output to produce an estimate of the bottom properties in a single step, although this single step may be quite computationally intensive. These methods are commonly known as matched-field inversion (MFI) [8] for the estimation of environmental parameters using matched-field techniques (also known as fullfield methods).

The Widely scalable Mobile Underwater Sonar Technology (WiMUST) project¹ proposes a new setup where the receivers are now short arrays towed by individual Autonomous Underwater Vehicles (AUVs). The AUVs, and therefore the receiving arrays, are free to move (almost) freely relative to each other and to the source. This movement freedom brings a new dimension to the problem by creating an effective Distributed Sensor Array (DSA). Whether this “freedom” allows to reach new gains in terms of performance and adaptivity for determining the sub-bottom structure in rapidly changing environments is a challenging question that is known to be both nonlinear and ill-conditioned, because it is scenario dependent and under constrained, with a high number of degrees of freedom.

In this work, this question is approached first by defining the concept of performance in the field of bottom inversion and then by applying that performance concept for comparing the two concurrent data models underlying the methodologies above: the reflection model normally used in seismic imaging and the acoustic propagation model used in MFI. The intention is to bridge this apparent gap between seismic profiling and MFI methods by proposing common performance criteria. These criteria will encompass topics such as processing gain, separation (resolution) of closely spaced layers and the detection of low reflectance layers.

This paper is organized as follows: the two data models are described in section II: a classical weighted sum of delayed signals and a full-field non-analytic model. Section III proposes performance criteria definitions where bottom inference is treated using a conventional power correlator. Results obtained on synthetic data and conclusions are given in sections IV and V, respectively.

¹funded by the H2020 European Union research programme under contract ICT-645141.

II. DATA MODEL

The data model assumes a linear source - receiver relation in additive noise, as

$$\begin{aligned} \mathbf{X} &= \mathbf{H}\mathbf{S} \\ \mathbf{Y} &= \mathbf{X} + \mathbf{U}, \end{aligned} \quad (1)$$

where \mathbf{X} is the noise free signal matrix of dimension $KN \times LN$ with K the number of sensors, L the number of source shots and N the number of time (or frequency) samples; \mathbf{S} is a square LN matrix containing the source shots

$$\mathbf{S} = \text{diag}[\mathbf{s}_1, \dots, \mathbf{s}_L], \quad (2)$$

where \mathbf{s}_l is a N -dimensional vector with the l -th source shot; the channel matrix \mathbf{H} is given by

$$\mathbf{H}_a = \begin{bmatrix} \mathbf{H}_{11} & \mathbf{H}_{12} & \dots & \mathbf{H}_{1L} \\ \mathbf{H}_{21} & \mathbf{H}_{22} & \dots & \mathbf{H}_{2L} \\ \vdots & \vdots & \ddots & \vdots \\ \mathbf{H}_{K1} & \mathbf{H}_{K2} & \dots & \mathbf{H}_{KL} \end{bmatrix}, \quad (3)$$

where each block represents the N -sample channel impulse response (CIR) h_{kl} , for sensor k and source shot l ; and \mathbf{U} is the noise component. In general the CIR contains the superposition of direct, surface and bottom reflected paths, or combinations of those, as they propagate along the water column and bounce from the various sub-bottom layers. This will be termed as the *full acoustic field* and is described below as seismo-acoustic propagation model (SPM). Isolate the reflections of a small bottom portion from the other acoustic arrivals, that are treated as noise, is generally the objective pursued in traditional seismic imaging that leads to the so-called seismic reflection model (SRM).

A. Seismic-reflection model (SRM)

This model assumes near vertical angle P-wave reflection where the signal travels through each layer suffering attenuation and specific speed variations with (as much as possible) limited angle of incidence deviations. Thus, according to the seismic reflection model (SRM), the received signal is a sum of weighted and time delayed replicas of the emitted signal reflected in the various bottom layers. Thus for sensor k and source shot l , the expected CIR is assumed to be

$$h_{kl}(t) = \sum_{m=1}^M a_{kl}(m) \delta[t - \tau_{kl}(m)], \quad (4)$$

where the weights $a_{kl}(m)$ are expected to be related the reflection coefficient and the delays $\tau_{kl}(m)$ to the depth of the respective reflector m . At near vertical incidence and under appropriate half hydrophone spacing array movement per source shot interval² the classical situation is sketched in Figure 1. This figure shows the traditional seismic processing for forming a Common Mid Point (CMP) gather, equivalent

²without loss of generality, sensor arrays are assumed linear equispaced for simplicity, even if that is not an absolute requirement in practice.

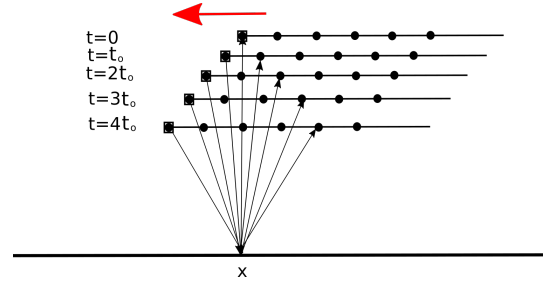


Fig. 1. (not to scale) sketch of trace gathering during typical seismic survey with a d -meter equispaced streamer advancing at speed $v = (d/2)/t_0$ in the direction of the red arrow, where t_0 is the source firing interval. The black square represents the sound source and the dots the receivers. The source is collocated with the first sensor.

to a delay and sum processing of sensor outputs. This corresponds to considering that the diagonal sub-matrices of matrix (3) are time-delayed replicas of each other. This is true for the main diagonal, and for all the other diagonals above and below the main diagonal (that correspond to other bottom locations before and after location “X”). The number of sub-matrices taken along each diagonal (gather fold) depend on a number of environmental and operational parameters. The operation along matrix (3) may be viewed as what is termed in the literature as the various gathers (see for example Figure 3.7, pp.24 of [9]). According to this model the noise matrix term \mathbf{U} contains not only electronic and ambient noise but also all the other acoustic returns from phenomena not accounted for in vertical reflection such as reflection multiples, refraction and S-waves, all characteristic of anisotropic elastic media..

B. Seismo-acoustic propagation model (SPM)

The model described in the previous section relies on bottom normal incidence of the acoustic wave and is, therefore, limited to a small number of snapshots within each time frame overlooking a given bottom bin. The achievable gain is therefore also limited, as it can be seen by the number of elements along the diagonals of sensing matrix (3) and geometric requirements referred to in the previous section. Increasing the sensor processing gain requires including more terms of matrix (3) and therefore opening up the observation angle from vertical to horizontal propagation. The methods that take into account the full wave field for bottom inversion are termed in the seismic literature as *Full Waveform Inversion* (FWI) (see [10] for recent examples and an excellent review in [11]).

A full seismo-acoustic propagation model (SPM) would allow, in principle, to appropriately treat the interaction between layers, according to its specific physical properties (if they are known or assumed). The acoustic received field at observation location \mathbf{r}_k due to a unit amplitude monochromatic point source located at \mathbf{r}_s may be written using the Green function $G(\cdot)$, solution of the Helmholtz equation between two points in space, as

$$G^E(\mathbf{r}_k, \mathbf{r}_s) = G^I(\mathbf{r}_k, \mathbf{r}_s) + G^R(\mathbf{r}_k, \mathbf{r}_s), \quad (5)$$

where G^E , G^I and G^R are the excitation, the incident and the reflected fields, respectively, all taken between the source located at \mathbf{r}_s and the receiver location \mathbf{r}_k . So the bottom reflected field excluding the direct field, is given as [12]

$$G^R(\mathbf{r}_k, \mathbf{r}_s) = \sum_{i=1}^I a_i G(\mathbf{r}_k, \mathbf{r}_i) G^I(\mathbf{r}_i, \mathbf{r}_s), \quad (6)$$

where $G(\mathbf{r}_k, \mathbf{r}_i)$ is the Green function between reflector located at bottom position \mathbf{r}_i and sensor at \mathbf{r}_k , $G^I(\mathbf{r}_i, \mathbf{r}_s)$ is the bottom incident field at \mathbf{r}_i from the sound source at location \mathbf{r}_s , a_i is a complex amplitude coefficient of the i -th reflector assumed random distributed and finally I is the number of effective reflectors. The Born approximation allows for the linearization of the interscatterer excitation field (the so-called Foldy-Lax system, see details in [13]) so the end result would be equivalent to (6). At this point our CIR in matrix \mathbf{H}_{kl} is given by the discrete inverse Fourier transform of the right hand side of (6) with the appropriate location vectors \mathbf{r}_k and \mathbf{r}_l defined for the k -th sensor and l -th source shot positions

$$h_{kl}(n) = \frac{1}{2\pi} \int_{\omega} \sum_{i=1}^I a_i G(\omega; \mathbf{r}_k, \mathbf{r}_i) G^I(\omega; \mathbf{r}_i, \mathbf{r}_l) e^{j\omega n T_s} d\omega, \quad (7)$$

where T_s is the sampling interval and the a_i are assumed frequency independent. Under the SPM assumption there is no implicit relation between the elements of the \mathbf{H} matrix, although the source-bottom-array geometry and the environmental physical parameters are known (or assumed known) at all times. The source-bottom-array geometry defines the contributing reflectors of the bottom spatial grid at each time, as the surveying system moves along.

III. PERFORMANCE AND OPTIMALITY

The criteria for performance comparison of the two data models above are normalized array gain, signal-to-noise ratio (SNR) gain, probability of detection and layer resolution, which are common to various areas of signal array processing with the difference that, in this case, the objective is the detection and estimation of layer interfaces into the ocean bottom. A power correlator (Bartlett) was used as array processor.

A. Normalized array gain

One way of assessing system overall performance is to see it as a filter adjusted for the assumed signal model. The ratio between the actual and the optimal SNR performance will give an indication of the expected performance,

$$|\Lambda|^2 = \frac{\rho(\boldsymbol{\theta}, \boldsymbol{\theta}_o)}{\rho_{\max}} \quad (8)$$

where $\rho(\boldsymbol{\theta}, \boldsymbol{\theta}_o)$ is the output SNR for parameter vector $\boldsymbol{\theta}$, when adjusted for $\boldsymbol{\theta}_o$. In our case $\boldsymbol{\theta}$ corresponds to depth z and $\boldsymbol{\theta}_o$

to actual depth z_o . For the SRM model this ratio is given by

$$|\Lambda_{\text{SRM}}|^2 = \frac{|\mathbf{s}^H \sum_{j=1}^J \mathbf{H}_{jj}^H(z_o) \mathbf{H}_{jj}(z) \mathbf{s}|^2}{\mathbf{s}^H \sum_{j=1}^J \mathbf{H}_{jj}^H(z_o) \mathbf{H}_{jj}(z_o) \mathbf{s} \mathbf{s}^H \sum_{j=1}^J \mathbf{H}_{jj}^H(z) \mathbf{H}_{jj}(z) \mathbf{s}}, \quad (9)$$

and for the SPM model by

$$|\Lambda_{\text{SPM}}|^2 = \frac{|\mathbf{s}^H \sum_{l=1}^L \sum_{k=1}^K \mathbf{H}_{kl}^H(z_o) \mathbf{H}_{kl}(z) \mathbf{s}|^2}{\mathbf{s}^H \sum_{l=1}^L \sum_{k=1}^K \mathbf{H}_{kl}^H(z) \mathbf{H}_{kl}(z) \mathbf{s} \mathbf{s}^H \sum_{l=1}^L \sum_{k=1}^K \mathbf{H}_{kl}^H(z_o) \mathbf{H}_{kl}(z_o) \mathbf{s}}. \quad (10)$$

Note that summation is done over J matrix diagonal terms of \mathbf{H} in (3) for SRM and for all KL matrix terms for SPM.

B. SNR gain

SNR gain is classically computed as the ratio between the output and input (mean) SNR as,

$$G_{\text{SNR}} = \frac{\rho(\boldsymbol{\theta}, \boldsymbol{\theta}_o)}{\bar{\rho}_{\text{in}}}, \quad (11)$$

where $\bar{\rho}_{\text{in}}$ is the mean input SNR over array sensors. For the SRM and SPM models, respectively

$$G_{\text{SRM}} = \begin{cases} K |\Lambda_{\text{SRM}}|^2, & J = K, K < L \\ \frac{\mathbf{s}^H \sum_{j=1}^J \mathbf{H}_{jj}^H(z_o) \mathbf{H}_{jj}(z) \mathbf{s}}{K |\Lambda_{\text{SRM}}|^2} & J = L, L < K, \\ \frac{\mathbf{s}^H \sum_{k=1}^K \mathbf{H}_k^H(z_o) \mathbf{H}_k(z) \mathbf{s}}{K |\Lambda_{\text{SRM}}|^2} & \end{cases} \quad (12)$$

with $|\Lambda_{\text{SRM}}|^2$ given by (9) and

$$G_{\text{SPM}} \approx \frac{K |\mathbf{s}^H \sum_{l=1}^L \sum_{k=1}^K \mathbf{H}_{kl}^H(z_o) \mathbf{H}_{kl}(z) \mathbf{s}|^2}{|\sum_{l=1}^L \sum_{n=0}^{N-1} |s(n)|^2 |\bar{h}(n)|^2| |\sum_{n=0}^{N-1} |s(n)|^2 |\bar{h}(n)|^2|}, \quad (13)$$

where the approximation in (13) consists on assuming that channel diversity over sensor is sufficient for the matrix product to become diagonal, where $\bar{h}(n)$ is the ‘‘mean’’ CIR. Therefore the double summation becomes the product of the sum of the diagonal terms.

C. Layer detection

Probability of detection is given by the classical expression $P_D = Q[Q^{-1}(P_{FA}) - \sqrt{d^2}]$, where Q is the Gaussian tail distribution function, P_{FA} is the probability of false alarm and $d^2 = \mathcal{E}_{x-\bar{x}}/\sigma_u^2$ is a measure of the SNR for the energy intersection between the received source signal x and the

expected signal \tilde{x} received from the reflector location. For the SRM model

$$\mathcal{E}_{x-\tilde{x}} \approx 2 \sum_{n=0}^{N-1} |s(n)|^2 |\bar{h}(n)|^2 - 2s^H \sum_{j=1}^J \mathbf{H}_{jj}^H(\theta_o^z) \mathbf{H}_{jj}(\theta^z) \mathbf{s}, \quad (14)$$

where, $J = \min(K, L)$ and the diagonalisation in the first term was done over J snapshots (or sensors). It is clear that when the mismatch is maximum, the second term is zero, and d^2 is maximum, and equal to the first term. Conversely, in the no mismatch case the second term is equal to the first term and d^2 is zero, or close to zero due to the approximations.

Instead, for the SPM model

$$\mathcal{E}_{x-\tilde{x}} \approx 2 \sum_{l=1}^L \sum_{n=0}^{N-1} |s(n)|^2 |h(n)|^2 - 2s^H \sum_{l=1}^L \sum_{k=1}^K \mathbf{H}_{kl}^H(\theta_o) \mathbf{H}_{kl}(\theta^r) \mathbf{s}, \quad (15)$$

where now the diagonalisation in the first term was done over K sensors. When $K \leq L$, we have $J = K$ in the SRM detection expression (14) and for the same degree of mismatch, $\mathcal{E}_{\text{SPM}} \approx L \mathcal{E}_{\text{SRM}}$, conversely if $L \leq K$ and $J = L$, then \mathcal{E}_{SPM} is even higher and $\approx K \mathcal{E}_{\text{SRM}}$. A higher cross energy means a higher SNR equivalent d^2 so, the detection probability P_D , as a function of SNR, moves towards lower SNR. Since this curve is monotonic, for a given SNR, P_D increases and the performance is higher. The conclusion is that, in theory, the detection probability of the SPM is higher than that of the SRM, for the same SNR and degree of mismatch.

D. Layer resolution

As explained above, layer resolution may be numerically deduced from the approximated expression

$$\Delta z_{\text{SRM/SPM}} = \arg_{z \in \mathbb{Z}} \left[P_{\text{SRM/SPM}}(z) = \frac{P_{\text{SRM/SPM}}(z_o)}{2} \right], \quad (16)$$

where $P_{\text{SRM/SPM}}$ is the Bartlett expression for models SRM/SPM. Analytical values can not be obtained since the side-lobe structure will depend on two factors: one is the bottom reflection structure present in the CIR cross-correlation and the other is the actual layer depth we are looking at, *i.e.*, the value of z_o . This is a phenomena similar to that observed in plane wave beamforming with linear arrays, where the main lobe width varies with the look direction (in this case the “look” depth).

IV. SIMULATION RESULTS

A. The Peljesac scenario

The simulation scenario is intended to mimic the environment of a geophysical survey carried out in June 2015 in the area of Peljesac (Croatia). The environmental parameters are shown in table I. In this canonical scenario the source

is considered to be explosive, located at 0.3m depth and emitting in the band 700 - 2000 Hz. The sensing system is a towed horizontal array located at the same depth of the source covering a range (or offset) from 0 to 100m, with 100 sensors at 1m uniform spacing. A stylized representation of the

Layer	Depth (m)	C_p (m/s)	C_s (m/s)	α_p (dB/ λ)	α_s (dB/ λ)	ρ (Kg/cm ³)
water		1500	0	0	0	1
sed 1	30	1550	130	0.1	1.7	1.49
sed 2	38	1700	350	0.8	2.0	1.88
half space	48	2500	900	0.01	0.01	2.4

TABLE I
PELJESAC CANONICAL SCENARIO OASES MODEL PARAMETERS:
 C_p -COMPRESSIONAL VELOCITY, C_s SHEAR VELOCITY, α_p
COMPRESSIONAL ATTENUATION, α_s SHEAR ATTENUATION AND ρ
DENSITY .

environmental description of the Peljesac canonical scenario is shown in Figure 2. The output of a transmission loss (TL)

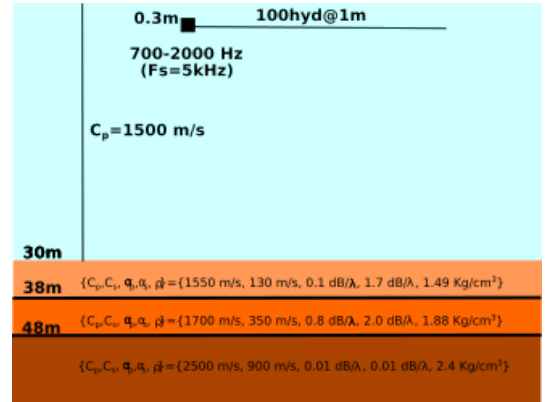


Fig. 2. OASES style environmental description for the canonical case scenario based on the Peljesac (Croatia, 2015) geophysical survey.

run at 1350 Hz, computed using OAST, the OASES [14] transmission loss propagation module, is shown in Figure 3 (a) and the CIR for the whole array length computed using the OASES pulse module, shown in (b). Several obvious remarks can be made: i) at high grazing angles (near vertical) bottom penetration is high and sound covers all the layers down to the sub-bottom half space; ii) at approximately 50 m range the half space cut-off angle is reached and the penetration reaches only the second bottom layer, this happens until approximately 80 m range; iii) beyond that range, most of the energy reaches only the first sediment layer that has approximately the same compressional sound speed than the water column, and then propagates through it, eventually bouncing back to the water column at longer ranges. In the time-range plot of Figure 3(b), the curvature of the bottom arrival structure can clearly be seen for variable offset. At close range the field is dominated by the direct-surface reflect paths. Due to the close distance to the surface, a dipole behavior is observed. This signal tends to attenuate with offset due to the canceling interference between the two signals when the time of arrival difference becomes

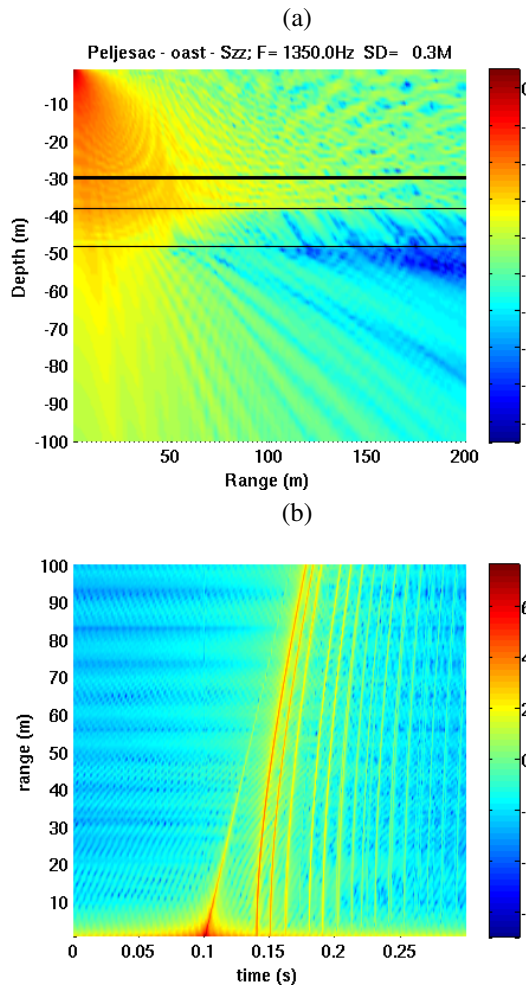


Fig. 3. transmission loss run at 1350 Hz using OAST (a) and CIR obtained for the band 700-2000 Hz using OASP in the Peljesac scenario (b).

of the order of the pulse width. This finite pulse width is, of course, due to the limited bandwidth.

B. Performance

Performance results are shown in Fig. 4 and table II for a $K = 8$ hydrophone array and $L = 8$ source shots, using the theoretical expressions of section III. Although a linear horizontal array was used, the same expressions may be used for any array geometry. At very close range (small offset), without mismatch and at vertical incidence the two models should follow very closely for the normalized criteria $|\Lambda|^2$. Since the acoustic model used in the SRM is, for this test, the same as that used in the SPM, the performance results end up being very similar with only a gain difference. In fact Fig 4 shows superimposed curves for the normalized array gain (a), where three peaks can be clearly identified for the three bottom interfaces at 30, 38 and 48 m depth, and a decay for deeper layers. A constant SNR gain difference of $20 \log 8 = 18$ dB is therefore observed in (b) with, also, a gain decrease for layers below 50 m depth. Probability of detection also slightly varies for each layer, in the correct order from L1

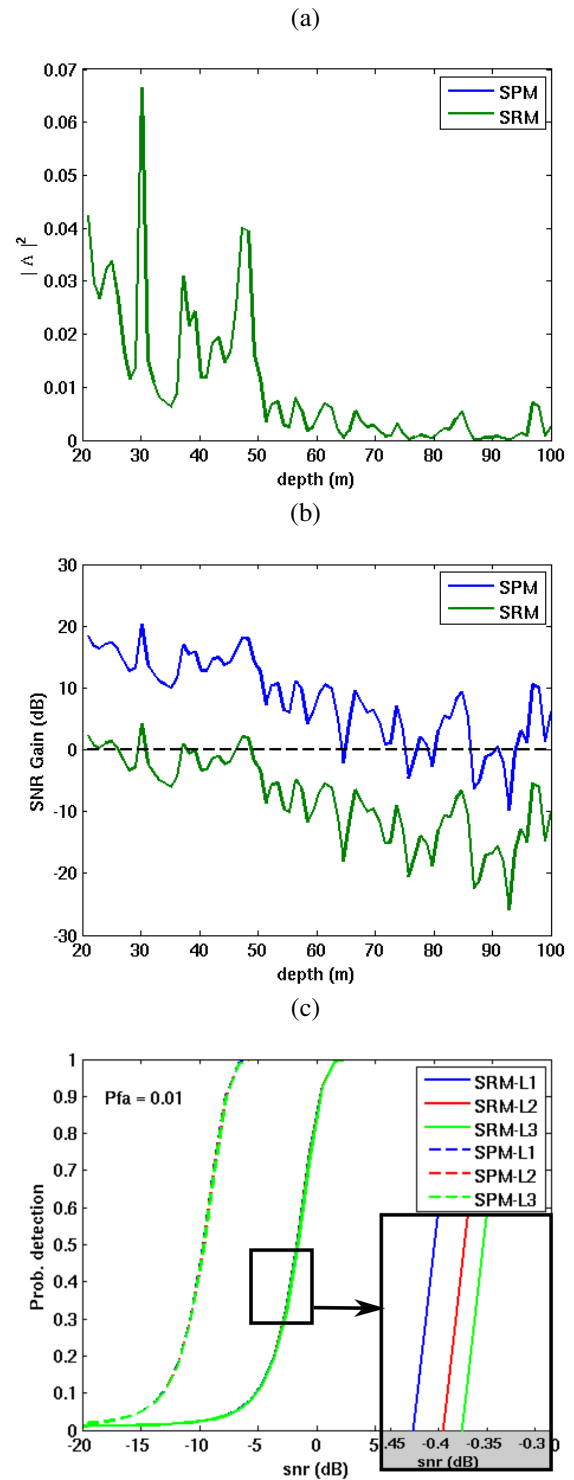


Fig. 4. performance indicators in the Peljesac scenario, 900-1400 Hz, $K = 8$ hydrophones, $L = 8$ source shots, without mismatch: normalized ratio $|\Lambda|^2$ (a), SNR gain (b) and probability of detection vs SNR for $P_{FA} = 0.01$ (c).

(shallower), L2 (intermediate) and L3 (deeper) with a clear performance difference of approximately 8 dB for a constant detection probability and a $P_{FA} = 0.01$, between the two models.

In terms of resolution, and as shown in table II the two

models provide very similar results with beamwidths of about 0.75, 3 and 4 meter for layers one (30m), two (38m) and three (48m), respectively, that, as expected, resolution decreases as depth increases.

Layer	depth (m)	Beam-width (-3 dB) (m)
sed 1	30	0.75
sed 2	38	~ 3
bottom	48	~ 4

TABLE II
RESOLUTION PERFORMANCE FOR THE SPM AND SRM MODELS IN THE PELJESAC CANONICAL SCENARIO USING OASES MODEL.

V. CONCLUSION

This work shows comparative performance results for two classical models used for bottom layering estimation. The two models correspond to the travel-time based direct reflection model (named here as SRM) traditionally used in seismic imaging and the fullfield propagation model used in matched-field inversion (dubed SPM in this paper). The fullfield model attempts to match not only directly bottom reflected waves but also reflected multiples, refracted and S-waves.

The assumptions made under each model lead to different processing techniques where for the SPM, the full ensemble of sensor - shot data is used whereas for the SRM, only the sensor-shots overlooking a given bottom bin within a given aperture are selected for processing. These restrictions are inherent to the delay-and-sum processing done in seismic imaging and are scenario dependent (bathymetry, array movement, sensor spacing, etc).

Four criteria have been used: normalized array gain, SNR gain, layer detection and layer resolution. These criteria are normally associated with the ability for each given model and setup to detect parameter changes, to provide SNR gain (and thus overall performance), to detect thin differences in bottom density and to resolve thin bottom layers. The results are illustrated for a scenario obtained from the area of Peljesac (Croatia) where a seismic survey took place in 2015. The results show that the normalized performance is identical for the two models in terms of layer identification and, as expected, sensitivity decreases with depth into the bottom. SNR gain will be normally higher for the SPM model since, in absence of mismatch, the number of data bins is also higher than for the SRM model. This gain difference reflects itself directly in a detection probability difference between the two models whereas the resolution is approximately the same.

The methodologies developed in this work are expected to provide operational tools for evaluating system performance in given scenarios and with variable array geometries prior to system deployment, thus based solely in apriori knowledge one may have about the area. This prediction will help in adapting system resources to a given desired performance/scenario, particularly useful for modular and scalable systems as those proposed under project WiMUST.

ACKNOWLEDGMENT

This work was funded under H2020 Research program of the European Union under project WiMUST contract ICT-645141. The authors thank multiple discussions with various colleagues of the WiMUST project namely with Henrique Duarte and Jonathan Grimsdale.

REFERENCES

- [1] O. Yilmaz, *Seismic data processing*. Tulsa: SEG, 1987.
- [2] R. Sheriff and L. Geldart, *Exploration Seismology*. Cambridge, UK: Cambridge university Press, 1995.
- [3] G. Frisk and J. Lynch, "Shallow water waveguide characterization using the hankel transform," *J. Acoust. Soc. America*, vol. 76, pp. 205–216, 1984.
- [4] G. Frisk, J. Lynch, and J. Douth, "The determination of geoaoustic models in shallow water," in *Ocean Seismo-Acoustics*, T. Akal and J. Berkson, Eds., Plenum, New York, 1986, pp. 998–1017.
- [5] M. Collins, W. Kuperman, and H. Schmidt, "Nonlinear inversion for ocean-bottom properties," *J. Acoust. Soc. America*, vol. 92, no. 5, pp. 2770–2783, November 1992. [Online]. Available: <http://dx.doi.org/10.1121/1.404394>
- [6] M. Siderius and J.-P. Hermand, "Yellow shark spring 1995: inversion results from sparse broadband acoustic measurements over a highly range-dependent soft clay layer," *J. Acoust. Soc. America*, vol. 106, no. 2, pp. 637–651, August 1999.
- [7] A. Caiti and S. Jesus, "Acoustic estimation of seafloor parameters: a radial basis functions approach," *J. Acoust. Soc. America*, vol. 100, no. 3, pp. 1473–1481, 1996.
- [8] Z.-H. Michalopoulou, "Robust multi-tonal matched-field inversion: A coherent approach," *J. Acoust. Soc. America*, vol. 104, pp. 163–170, 1998.
- [9] G. Drijkoningen and D. Verschuur, *Seismic data processing (TA3600/TG001)*, Centre for Technical Geoscience, Delft university of Technology, P.O. Box 5028, 2600 GA Delft, The Netherlands, 2003.
- [10] J. Brittan, J. Bai, H. Delome, C. Wang, and D. Yingst, "full waveform inversion - the state of the art," *EAGE First Break*, vol. 31, pp. 75–81, October 2013.
- [11] J. Virieux and S. Operto, "An overview of full-waveform inversion in exploration geophysics," *Geophysics*, vol. 74, no. 6, pp. WCC1–WCC26, November-December 2009. [Online]. Available: <http://dx.doi.org/10.1190/1.3238367>
- [12] A. Fannjiang, P. Yann, and T. Strohmer, "Compressed remote sensing of sparse objects," *arXiv:0904.3994*, 2009.
- [13] K. Huang, K. Solna, and H. Zhao, "Generalized Foldy-Lax formulation," *J. Comput. Physics*, vol. 229, pp. 4544–4553, 2010.
- [14] H. Schmidt, *OASES 3.1 - User guide and reference manual*, MIT, March 2011.